J Mater Sci (2008) 43:3510–3521
DOI 10.1007/s10853-008-2479-3

Effective properties of materials with random micro-cavities using special boundary elements

Federico C. Buroni · Rogério J. Marczak

Received: 24 April 2007 / Accepted: 18 January 2008 / Published online: 23 March 2008

Abstract In this work, a general boundary element procedure is proposed to obtain the effective elastic tensor of solids containing randomly distributed micro-cavities in terms of its primary elastic properties. The average-field theory and a special boundary element formulation are combined to carry out a statistical analysis on the numerical results obtained for a Representative Volume Element (RVE). The two-dimensional isotropic material is simulated as a homogeneous matrix containing cylindrical holes. In the proposed implementation each hole boundary is modeled with a single boundary element. The average variables of the micro-field are evaluated using boundary-only data, which leads to a formulation particularly suitable for Boundary Element Methods. Expressions for effective elastic properties as a function of the micro-fields for both isotropic and transversally isotropic hypothesis are derived. Finally, the methodology is illustrated with some application examples and the results are compared with analytical and experimental results.

Introduction

Engineering materials, like everything in Nature, are heterogeneous when observed at a certain scale. The determination of macroscopic characteristics of heterogeneous materials is an essential problem in many applications of engineering and science. The study of relationships between microstructural phenomenon and the macroscopic behavior not only allows predicting the behavior of existing materials, but also provides a tool for the designing microstructures such that the resulting macroscopic behavior meets the desired characteristics.

Currently, the use of numerical methods to solve differential equations such as the Finite Element Method (FEM) and the Boundary Element Method (BEM) is fully generalized. The combination of micromechanics and such numerical methods supplies a powerful tool for modeling material behavior [1]. The BEM has already shown to be very accurate and efficient when compared to other popular methods for many problems in Solids Mechanics. In particular, the BEM can perform quite efficiently [2] in overall properties predictions, since the spatial average scheme of internal fields of the variables requires only data from the microstructure boundary [3–8]. This work is addressed to micro-porous materials consisting of an isotropic and homogeneous matrix containing randomly distributed cylindrical voids. In order to predict the linearly elastic response of the material, a statistical analysis scheme is used with the Effective Property Theory (also called Average-Field Theory) [9, 10]. The theory predicts the effective properties of a macroscopic sample of the material based on the volume average of the stress field extracted from micro-heterogeneous samples. Therefore, macro-fields are defined as volume averages of the corresponding micro-fields, and the effective properties are determined from relationships between the averaged micro-fields [10, 11]. The analysis must be accomplished on a representative sample of material so that it incorporates a sufficient amount of micro-voids, known in the literature as Representative Volume Element (RVE).

F. C. Buroni · R. J. Marczak (✉)
Department of Mechanical Engineering, Federal University of Rio Grande do Sul, Rua Sarmento Leite 425, 90050-170 Porto Alegre, RS, Brazil
e-mail: rato@mecanica.ufrgs.br

F. C. Buroni
e-mail: fedeburoni@yahoo.com.br

In this work a general procedure to predict the effective elastic tensor of random micro-porous materials is presented. A boundary element formulation [12, 13] is used to model two-dimensional micro-structured material samples. The formulation includes a family of special elements [14] that allow the modeling of each micro-void as a single special *hole element*. The microstructure discretization strategy becomes simply the indication of the center of each void, its radius and the element order, besides the conventional outer boundary element mesh. Therefore the amount of data and computational cost is considerably reduced, and the discretization becomes simpler than the conventional BEM or other methods (Fig. 1a). In addition, a static condensation scheme [13] can be applied in order to reduce the size of the system of equations. This is a welcome characteristic when the numerical analysis of the RVE has to be performed many times such as during the design phase of a new material or in the assessment of an existing one within a statistical degree of confidence. Expressions for effective properties as functions of the micro-fields under both isotropic and transversally isotropic hypothesis are derived. The developed numerical tool is illustrated with some application examples.

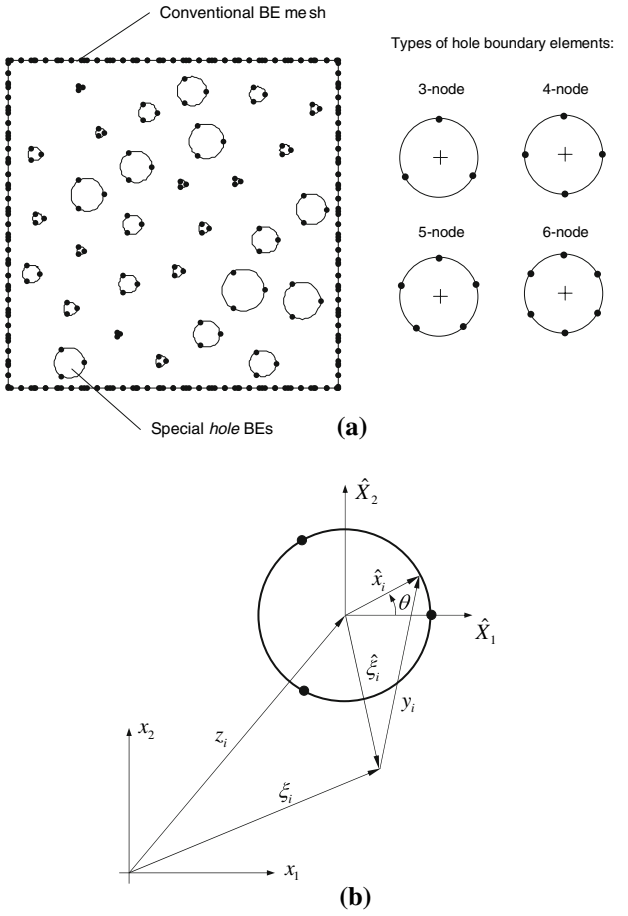

Fig. 1 (**a**) Special *hole* elements used in this work. (**b**) Local and global reference system in a 3-noded hole element

Numerical modeling of material

In this section, the BEM formulation employed herein is briefly summarized. For details the reader can be refer [12–15].

Boundary integral formulation for a matrix containing cylindrical holes

The direct boundary integral equation for displacements [16] of an elastic solid can be applied to solve the boundary value problem of a microstructure with domain Ω surrounded by an outer boundary Γ_o, containing cylindrical micro-holes with boundary Γ. For each hole, a local coordinate system $\widehat{X}_i$ is defined with its origin coincident with the hole center. The notation $\widehat{(\cdot)}$ is used to refer variables in the local system. The origin of the local system in the global co-ordinate system x_i is determined by the vectors z_i, while the axis $\widehat{X}_i$ are kept parallel to x_i as is indicated in Fig. 1b. Thus, a particular hole boundary point $\widehat{x}_i$ can be expressed as:

$$\begin{aligned} \widehat{x}_1 &= R\cos\theta \\ \widehat{x}_2 &= R\sin\theta \end{aligned} \tag{1}$$

where R is the radius of the hole. The components of normal vector at $\widehat{x}_i$ are expressed by:

$$\begin{aligned} \widehat{n}_1 &= -\cos\theta \\ \widehat{n}_2 &= -\sin\theta \end{aligned} \tag{2}$$

The boundary integral equation for the problem of a matrix containing N_f cylindrical holes without internal pressure and in absence of body force is given by [12–14]:

$$\begin{aligned} \mathsf{C}_{ij}(\xi)u_i(\xi) = &\int_{\Gamma_o}\left[G^o_{ij}(x,\xi)t^o_i(x) - F^o_{ij}(x,\xi)u^o_i(x)\right]\mathrm{d}\Gamma \\ &- \sum_{n=1}^{N_f}\int_{2\pi}^{0}\widehat{F}^{f}_{ij}\left(R,\theta,\widehat{\xi}\right)u^f_i(\theta)R_n\mathrm{d}\theta \end{aligned} \tag{3}$$

where i, j denote Cartesian components, u_i and t_i are the boundary displacements and tractions, G_{ij} and F_{ij} are the Kelvin fundamental solution at a point ξ due to the unit load placed at location x, and $\mathsf{C}_{ij}(\xi)$ are the geometric factors of the boundary point ξ. The superscripts o and f (no sum) refer to the quantities on the outer boundary of the matrix and on the holes' boundaries, respectively. Analytical expressions for the tensor $\widehat{F}^{f}_{ij}$ in the reference system $\widehat{X}_i$ can be found in reference [15] for the plane stress and plane strain hypothesis.

In order to numerically solve Eq. 3, the outer material matrix boundary Γ_o is discretized with discontinuous quadratic elements. The displacements field on the boundary of the hole Γ is interpolated with special shape functions M_i so that each of those is modeled with a single element. Trigonometric functions are used as base for the element shape functions resulting in elements with 3, 4, 5, and 6 nodes [14]. The shape functions of these elements are presented in the Appendix. The displacement boundary integral equation for the nth hole boundary Γ^n interpolated using such functions is found to be:

$$\int_{\Gamma^n} F_{ij}^{\mathrm{f}}(x,\xi)u_i^{\mathrm{f}}(x)\mathrm{d}\Gamma = U_i^{\beta}\int_{2\pi}^{0}\widetilde{F}_{ij}^{\mathrm{f}}\left(R,\theta,\widetilde{\xi}\right)M_{\beta}(\theta)R\mathrm{d}\theta \tag{4}$$

where U_i^{β} are the displacements of the node β in the direction i and β range from 1 to the number of nodes of the element. The integral in Eq. 4 contains strongly singular kernels which are directly evaluated resulting a regularized hole element [15].

Once the collocation of the boundary integral equation for each nodal point is preformed, a linear system of equations results. After the imposition of the boundary conditions, the system can be solved to provide the approximate field of the unknowns on the boundary [17].

Contrary to the conventional BEM, which would require a fine meshing for each hole, the present approach allows an efficient analysis, reducing significantly the input data amount and the total number of degree of freedom without compromising the overall accuracy. This is particularly important in the analysis of material samples containing hundreds or thousands of voids [18]. Note that a RVE FEM analysis for high number of holes would waste a huge amount of computational resources, since the results for internal nodes play no direct role in effective properties estimation, not to mention the overhead implied in mesh generation.

Computational modeling of the material

Computational test of the material

The evaluation of the macroscopic elastic properties C_{ijkm}^{*} of a heterogeneous material relies on the computation of the following relationship between averages on the sample volume Ω [9, 10]:

$$\langle\sigma_{ij}\rangle_{\Omega} = C_{ijkm}^{*}\langle\varepsilon_{km}\rangle_{\Omega} \tag{5}$$

or, using Voigt's notation:

$$\begin{Bmatrix}\langle\sigma_{11}\rangle_{\Omega}\\ \langle\sigma_{22}\rangle_{\Omega}\\ \langle\sigma_{33}\rangle_{\Omega}\\ \langle\sigma_{23}\rangle_{\Omega}\\ \langle\sigma_{13}\rangle_{\Omega}\\ \langle\sigma_{12}\rangle_{\Omega}\end{Bmatrix} = \begin{bmatrix}c_{11}^{*} & c_{12}^{*} & c_{13}^{*} & c_{14}^{*} & c_{15}^{*} & c_{16}^{*}\\ c_{21}^{*} & c_{22}^{*} & c_{23}^{*} & c_{24}^{*} & c_{25}^{*} & c_{26}^{*}\\ c_{31}^{*} & c_{32}^{*} & c_{33}^{*} & c_{34}^{*} & c_{35}^{*} & c_{36}^{*}\\ c_{41}^{*} & c_{42}^{*} & c_{43}^{*} & c_{44}^{*} & c_{45}^{*} & c_{46}^{*}\\ c_{51}^{*} & c_{52}^{*} & c_{53}^{*} & c_{54}^{*} & c_{55}^{*} & c_{56}^{*}\\ c_{61}^{*} & c_{62}^{*} & c_{63}^{*} & c_{64}^{*} & c_{65}^{*} & c_{66}^{*}\end{bmatrix}\begin{Bmatrix}\langle\varepsilon_{11}\rangle_{\Omega}\\ \langle\varepsilon_{22}\rangle_{\Omega}\\ \langle\varepsilon_{33}\rangle_{\Omega}\\ 2\langle\varepsilon_{23}\rangle_{\Omega}\\ 2\langle\varepsilon_{13}\rangle_{\Omega}\\ 2\langle\varepsilon_{12}\rangle_{\Omega}\end{Bmatrix} \tag{6}$$

where $\langle\cdot\rangle_{\Omega}\overset{def}{=}\frac{1}{|\Omega|}\int_{\Omega}\cdot\mathrm{d}\Omega$ is the spatial average operator, and σ_{ij} and ε_{ij} are the stress and strain micro-fields within the material sample, respectively. In order to Eq. 6 remain valid, it must be applied necessarily on a RVE [9, 10]. Then, the microstructure can be computationally tested to extract the stress and the strain micro-fields. The constants of the elastic matrix are obtained solving the system of equations (6). The sample of micro-structured material is submitted to the same boundary conditions that would generate uniform stress or strain fields in a homogeneous body. Linear displacements conditions $u_i|_{\Gamma} = \mathcal{E}_{ij}x_j$ or uniform tractions $t_i|_{\Gamma} = \mathcal{L}_{ij}n_j$ along the boundary of the outer material matrix are generally considered, with constant $\mathcal{E}_{ij}$ and $\mathcal{L}_{ij}$. The most commonly used set of linearly independent load cases are:

$$\mathcal{L},\mathcal{E} = \begin{bmatrix}\beta & 0 & 0\\ 0 & 0 & 0\\ 0 & 0 & 0\end{bmatrix},\begin{bmatrix}0 & 0 & 0\\ 0 & \beta & 0\\ 0 & 0 & 0\end{bmatrix},\begin{bmatrix}0 & 0 & 0\\ 0 & 0 & 0\\ 0 & 0 & \beta\end{bmatrix},\begin{bmatrix}0 & \beta & 0\\ \beta & 0 & 0\\ 0 & 0 & 0\end{bmatrix},\begin{bmatrix}0 & 0 & \beta\\ 0 & 0 & 0\\ \beta & 0 & 0\end{bmatrix},\begin{bmatrix}0 & 0 & 0\\ 0 & 0 & \beta\\ 0 & \beta & 0\end{bmatrix} \tag{7}$$

where β is a constant load parameter. Each one of the six independent load cases supplies six equations for a total of 36 equations from which the elastic constants in Eq. 6 can be retrieved.

Effective properties of micro-porous materials

Some simplifications are assumed in the micro-structure model. First, the microstructure consists of a homogeneous and isotropic matrix containing randomly distributed micro-voids. Each micro-void is considered cylindrical and with traction-free boundary. No micro-structural changes are allowed to happen within the load application history (such as the nucleation and/or coalescence of micro-voids or phase transformations in the matrix). Under these assumptions, an explicit analysis is possible by considering only the final load state. The response of the model is limited to linear elastic behavior with infinitesimal strain in the macro as well as in the micro-scale.

Since the effective properties of the material are computed as indicated in "Computational test of the material"

section, it is necessary obtain the average fields $\langle\sigma_{ij}\rangle_\Omega$ and $\langle\varepsilon_{ij}\rangle_\Omega$ in the micro-structure. In order to satisfy the Hill's energy condition, the boundary condition must be of linear displacement $u_i|_\Gamma = \mathcal{E}_{ij}x_j$ or uniform traction $t_i|_\Gamma = \mathcal{L}_{ij}n_j$ [2]. It is numerically cumbersome to impose a traction-only condition along the whole boundary in an explicit BEM formulation, and therefore the linear displacements case is considered here (in the absence of body forces this is sufficient to guarantee the satisfaction of the Hill's condition). Furthermore, after the average strain theorem, the strain field is recovered straightforwardly by $\langle\varepsilon\rangle_\Omega = \mathcal{E}$ [10].

In BEM, the unknowns are initially evaluated on the boundary, while the results at interior points are evaluated as a post-processing stage. A simple way to evaluate the RHS of Eq. 5 using boundary-only data is outlined below.

Departing from the third-order tensor definition $\sigma \otimes x \overset{def}{=} \sigma_{ij}x_k$ one has:

$$\left(\sigma_{ij}x_k\right)_{,j} = \sigma_{ij,j}x_k + \sigma_{ij}x_{k,j} = \sigma_{ij,j}x_k + \sigma_{ij}\delta_{kj} = \sigma_{ij,j}x_k + \sigma_{ik} \tag{8}$$

and using the equilibrium equations of elasticity results:

$$\left(\sigma_{ij}x_k\right)_{,j} = -b_ix_k + \sigma_{ik} \Rightarrow \sigma_{ik} = \left(\sigma_{ij}x_k\right)_{,j} + b_ix_k \tag{9}$$

Recalling the requirement of body forces absence, the stress tensor field can be expressed as $\sigma_{ik} = (\sigma_{ij}x_k)_{,j}$, so that the average stress is written as [9]:

$$\langle\sigma_{ij}\rangle_\Omega = \frac{1}{|\Omega|}\int_\Omega \left(\sigma_{ik}x_j\right)_{,k} \mathrm{d}\Omega \tag{10}$$

where $|\Omega|$ considers the total volume of the matrix and the voids as well. Applying the Green's theorem to Eq. 10, it is easily taken to the boundary:

$$\langle\sigma_{ij}\rangle_\Omega = \frac{1}{|\Omega|}\int_{\Gamma_o} \sigma_{ik}x_jn_k \mathrm{d}\Gamma \tag{11}$$

and the integration is performed over the outer boundary of the micro-structure Γ_0 since the voids are stress free.

Considering that the boundary Γ_o is discretized with discontinuous quadratic elements, Eq. 11 can be rewritten using the boundary traction data and the element shape functions, yielding:

$$\langle\sigma_{ij}\rangle_\Omega = \frac{1}{|\Omega|}\sum_{k=1}^{\mathrm{NE}}\left\{\begin{bmatrix} T_i^1 & T_i^2 & T_i^3 \end{bmatrix}_k \int_{-1}^{1}\begin{bmatrix} \bar{\phi}_1(\eta)\phi_1(\eta) & \bar{\phi}_1(\eta)\phi_2(\eta) & \bar{\phi}_1(\eta)\phi_3(\eta) \\ \bar{\phi}_2(\eta)\phi_1(\eta) & \bar{\phi}_2(\eta)\phi_2(\eta) & \bar{\phi}_2(\eta)\phi_3(\eta) \\ \bar{\phi}_3(\eta)\phi_1(\eta) & \bar{\phi}_2(\eta)\phi_3(\eta) & \bar{\phi}_3(\eta)\phi_3(\eta) \end{bmatrix} J d\eta \begin{bmatrix} x_j^1 \\ x_j^2 \\ x_j^3 \end{bmatrix}_k\right\} \tag{12}$$

where NE is the number of elements on the boundary Γ_o, T_i^j and x_i^j are the ith traction and coordinate components of the jth local node of the kth element, respectively. ϕ_i and $\bar{\phi}_i$ stands for the geometric (quadratic) and physical (modified quadratic) element shape functions [17], while J is the Jacobian of the transformation to the normalized space $\eta = [-1, +1]$. In the numerical implementation of the present work, these integrals can be accurately computed with standard Gauss–Legendre quadrature using three Gauss's points. Note that the BEM is particularly suitable for computing effective properties by Eq. 11 since the only necessary data are the boundary tractions (or displacements). These are primal variables of the formulation and are obtained with great accuracy when compared with other methods.

Expressions for effective Young's modulus and Poisson's ratio in two-dimensions

Plane elasticity assumes hypothesis about the behavior in the third dimension (x_3), leading to the well-known models of plane strain and plane stress state. Therefore, it is possible to model a thin plate containing circular holes under plane stress hypothesis or a solid containing long cylindrical holes parallel to the x_3 as a plane strain case [10]. When the micro-constituents of the material are isotropic, the geometric symmetry of the microstructure implies macroscopic symmetry of the material. In a two-dimensional model, the x_3-plane must be a symmetry plane of the material. Taking this into account and considering the inhomogeneity of the microstructure, the most general case of the anisotropy which can be considered is monoclinic symmetry (in three dimensions). That symmetry is characterized by 13 independent elastic constants. If ones considers an in-plane anisotropy (also named transversally anisotropic or monoclinic material in three-dimensional elasticity), three load cases are needed in order to recover the elastic constants which determine the in-plane macroscopic behavior. The following cases are considered here:

$$\begin{Bmatrix} \langle\sigma_{11}\rangle_\Omega \\ \langle\sigma_{22}\rangle_\Omega \\ \langle\sigma_{12}\rangle_\Omega \end{Bmatrix} = \begin{bmatrix} c_{11}^* & c_{12}^* & c_{16}^* \\ c_{21}^* & c_{22}^* & c_{26}^* \\ c_{61}^* & c_{62}^* & c_{66}^* \end{bmatrix} \begin{Bmatrix} \beta \\ 0 \\ 0 \end{Bmatrix} \rightarrow \begin{cases} c_{11}^* = \frac{\langle\sigma_{11}\rangle_\Omega}{\beta} \\ c_{21}^* = \frac{\langle\sigma_{22}\rangle_\Omega}{\beta} \\ c_{61}^* = \frac{\langle\sigma_{12}\rangle_\Omega}{\beta} \end{cases} \tag{13}$$

$$\begin{Bmatrix} \langle\sigma_{11}\rangle_\Omega \\ \langle\sigma_{22}\rangle_\Omega \\ \langle\sigma_{12}\rangle_\Omega \end{Bmatrix} = \begin{bmatrix} c_{11}^* & c_{12}^* & c_{16}^* \\ c_{21}^* & c_{22}^* & c_{26}^* \\ c_{61}^* & c_{62}^* & c_{66}^* \end{bmatrix} \begin{Bmatrix} 0 \\ \beta \\ 0 \end{Bmatrix} \rightarrow \begin{cases} c_{12}^* = \frac{\langle\sigma_{11}\rangle_\Omega}{\beta} \\ c_{22}^* = \frac{\langle\sigma_{22}\rangle_\Omega}{\beta} \\ c_{62}^* = \frac{\langle\sigma_{12}\rangle_\Omega}{\beta} \end{cases} \tag{14}$$

$$\begin{Bmatrix} \langle\sigma_{11}\rangle_\Omega \\ \langle\sigma_{22}\rangle_\Omega \\ \langle\sigma_{12}\rangle_\Omega \end{Bmatrix} = \begin{bmatrix} c_{11}^* & c_{12}^* & c_{16}^* \\ c_{21}^* & c_{22}^* & c_{26}^* \\ c_{61}^* & c_{62}^* & c_{66}^* \end{bmatrix} \begin{Bmatrix} 0 \\ 0 \\ 2\beta \end{Bmatrix} \rightarrow \begin{cases} c_{16}^* = \frac{\langle\sigma_{11}\rangle_\Omega}{2\beta} \\ c_{26}^* = \frac{\langle\sigma_{22}\rangle_\Omega}{2\beta} \\ c_{66}^* = \frac{\langle\sigma_{12}\rangle_\Omega}{2\beta} \end{cases} \tag{15}$$

and the nine elastic constants of the plane can be obtained. Note that the symmetry of the elastic constant matrix is not taken into account.

In the case of the material studied here, the random distribution of holes in the plane (x_1, x_2) leads to a statistically isotropic behavior and the overall response in a RVE results a transversally isotropic symmetry, either for plane stress or plane strain models. With in-plane isotropy hypothesis, the elastic constant matrices are given as functions of the effectives Young's modulus E^* and the Poisson's ratio v^*. For plane stress and plane strain they are found to be, respectively:

$$\mathbf{C}_{\mathrm{PT}}^* = \frac{E^*}{1-v^{*2}} \begin{bmatrix} 1 & v^* & 0 \\ v^* & 1 & 0 \\ 0 & 0 & \frac{(1-v^*)}{2} \end{bmatrix} \tag{16}$$

and

$$\mathbf{C}_{\mathrm{PS}}^* = \frac{E^{*2}E_3^*}{(1+v^*)\{(1-v^*)E_3^* - 2v_3^{*2}E^*\}} \begin{bmatrix} \frac{1}{E^*} - \frac{v_3^{*2}}{E_3^*} & \frac{v^*}{E^*} + \frac{v_3^{*2}}{E_3^*} & 0 \\ \frac{v^*}{E^*} + \frac{v_3^2}{E_3^*} & \frac{1}{E^*} - \frac{v_3^{*2}}{E_3^*} & 0 \\ 0 & 0 & \frac{\{(1-v^*)E_3^* - 2v_3^{*2}E^*\}}{2E^*E_3^*} \end{bmatrix} \tag{17}$$

where E_3^* is the effective Young's modulus in the x_3-direction while the effective Poisson's ratio v_3^* is the normal deformation in any in-plane direction due to a stress in x_3-direction. It is interesting to note that in the plane strain model the in-plane behavior is a function of the response in the third dimension, which should be assumed. This does not happen in the plane stress model, where the constitutive law is the same of the isotropic case. Therefore, the in-plane constitutive law for the transversally isotropic material is characterized by two elastic constants and a single load case is sufficient to determine the overall response. However, there are two situations that do not allow the evaluation of these unknowns. If the boundary conditions are subjected to pure shear (for example, $\mathcal{E} = \lfloor 0 \quad 0 \quad 2\beta \rfloor^{\mathrm{T}}$), or a hydrostatic state ($\mathcal{E} = \lfloor \beta \quad \beta \quad 0 \rfloor^{\mathrm{T}}$), the system of equations resulting from the relationship between averages does not have a solution. This means that the boundary conditions must have non-null spherical and deviatoric components. It is also worth to note that this requirement refers to a plane domain and it is not considered a three-dimensional spherical or deviatoric state.

The expressions for E^* and v^* for a transversely isotropic material now can be derived from the system of equations (6) and the constitutive matrices (16) and (17). The following expressions are obtained:

$$\mathcal{E} = \lfloor \beta \quad 0 \quad 0 \rfloor^{\mathrm{T}} \rightarrow \begin{cases} E^* = \dfrac{1 - \left(\frac{\langle\sigma_{22}\rangle_\Omega}{\langle\sigma_{11}\rangle_\Omega}\right)^2}{\beta} \langle\sigma_{11}\rangle_\Omega \\ v^* = \dfrac{\langle\sigma_{22}\rangle_\Omega}{\langle\sigma_{11}\rangle_\Omega} \end{cases} \tag{18}$$

$$\mathcal{E} = \lfloor 0 \quad \beta \quad 0 \rfloor^{\mathrm{T}} \rightarrow \begin{cases} E^* = \dfrac{1 - \left(\frac{\langle\sigma_{11}\rangle_\Omega}{\langle\sigma_{22}\rangle_\Omega}\right)^2}{\beta} \langle\sigma_{22}\rangle_\Omega \\ v^* = \dfrac{\langle\sigma_{11}\rangle_\Omega}{\langle\sigma_{22}\rangle_\Omega} \end{cases} \tag{19}$$

for plane stress, and

$$\mathcal{E} = \lfloor \beta \quad 0 \quad 0 \rfloor^{\mathrm{T}} \rightarrow \begin{cases} E^* = \dfrac{4E_3^*\left(\langle\sigma_{11}\rangle_\Omega + \langle\sigma_{22}\rangle_\Omega\right)\beta^2}{\Xi_1\left(\langle\sigma_{11}\rangle_\Omega - \langle\sigma_{22}\rangle_\Omega\right)} \\ v^* = \dfrac{4E_3^*\beta\langle\sigma_{22}\rangle_\Omega - \langle\sigma_{11}\rangle_\Omega^2 v_3^* + \langle\sigma_{22}\rangle_\Omega^2 v_3^{*2}}{\Xi_1} \end{cases} \tag{20}$$

$$\mathcal{E} = \lfloor 0 \quad \beta \quad 0 \rfloor^{\mathrm{T}} \rightarrow \begin{cases} E^* = \dfrac{4E_3^*\left(\langle\sigma_{22}\rangle_\Omega + \langle\sigma_{11}\rangle_\Omega\right)\beta^2}{\Xi_2\left(\langle\sigma_{22}\rangle_\Omega - \langle\sigma_{11}\rangle_\Omega\right)} \\ v^* = \dfrac{4E_3^*\beta\langle\sigma_{11}\rangle_\Omega - \langle\sigma_{22}\rangle_\Omega^2 v_3^* + \langle\sigma_{11}\rangle_\Omega^2 v_3^{*2}}{\Xi_2} \end{cases} \tag{21}$$

for plane strain state, where the following definitions are used:

$$\Xi_1 = \beta\langle\sigma_{11}\rangle_\Omega E_3^* - 3\beta\langle\sigma_{22}\rangle_\Omega E_3^* + \langle\sigma_{11}\rangle_\Omega^2 v_3^* - \langle\sigma_{22}\rangle_\Omega^2 v_3^* \tag{22}$$

$$\Xi_2 = \beta\langle\sigma_{22}\rangle_\Omega E_3^* - 3\beta\langle\sigma_{11}\rangle_\Omega E_3^* + \langle\sigma_{22}\rangle_\Omega^2 v_3^* - \langle\sigma_{11}\rangle_\Omega^2 v_3^* \tag{23}$$

It is known that in homogeneous solids containing traction-free cavities parallel to the x_3-direction, E_3^* decreases with the volume fraction of the material, while v_3^* remains the same of the matrix [10]. It is interesting to rewrite the expressions (20–23) for micro-porous materials as a function of matrix properties and volume fraction ϕ:

$$\mathcal{E} = \lfloor \beta \quad 0 \quad 0 \rfloor^{\mathrm{T}} \rightarrow \begin{cases} E^* = \dfrac{4E_m(1-\phi)\left(\langle\sigma_{11}\rangle_\Omega + \langle\sigma_{22}\rangle_\Omega\right)\beta^2}{\Xi_1\left(\langle\sigma_{11}\rangle_\Omega - \langle\sigma_{22}\rangle_\Omega\right)} \\ v^* = \dfrac{4E_m(1-\phi)\beta\langle\sigma_{22}\rangle_\Omega - \langle\sigma_{11}\rangle_\Omega^2 v_m + \langle\sigma_{22}\rangle_\Omega^2 v_m^2}{\Xi_1} \end{cases} \tag{24}$$

$$\mathcal{E} = \lfloor 0 \quad \beta \quad 0 \rfloor^{\mathrm{T}} \rightarrow \begin{cases} E^* = \dfrac{4E_m(1-\phi)\left(\langle\sigma_{22}\rangle_\Omega + \langle\sigma_{11}\rangle_\Omega\right)\beta^2}{\Xi_2\left(\langle\sigma_{22}\rangle_\Omega - \langle\sigma_{11}\rangle_\Omega\right)} \\ v^* = \dfrac{4E_m(1-\phi)\beta\langle\sigma_{11}\rangle_\Omega - \langle\sigma_{22}\rangle_\Omega^2 v_m + \langle\sigma_{11}\rangle_\Omega^2 v_m^2}{\Xi_2} \end{cases} \tag{25}$$

where

$$\Xi_1 = \beta\langle\sigma_{11}\rangle_\Omega E_m(1-\phi) - 3\beta\langle\sigma_{22}\rangle_\Omega E_m(1-\phi) + \langle\sigma_{11}\rangle_\Omega^2 v_m - \langle\sigma_{22}\rangle_\Omega^2 v_m \tag{26}$$

$$\Xi_2 = \beta\langle\sigma_{22}\rangle_\Omega E_m(1-\phi) - 3\beta\langle\sigma_{11}\rangle_\Omega E_m(1-\phi) + \langle\sigma_{22}\rangle_\Omega^2 v_m - \langle\sigma_{11}\rangle_\Omega^2 v_m \tag{27}$$

In the plane strain isotropic case, the expressions for recovering the effective properties can be obtained setting $E_3 = E^*$ and $v_3 = v^*$:

$$\mathcal{E} = \lfloor \beta \quad 0 \quad 0 \rfloor^{\mathrm{T}} \rightarrow \begin{cases} E^* = \dfrac{\left(3\langle\sigma_{22}\rangle_\Omega - \langle\sigma_{11}\rangle_\Omega\right)}{\left(\langle\sigma_{22}\rangle_\Omega - \langle\sigma_{11}\rangle_\Omega\right)\beta}\langle\sigma_{11}\rangle_\Omega \\ v^* = -\dfrac{\langle\sigma_{22}\rangle_\Omega}{\langle\sigma_{22}\rangle_\Omega - \langle\sigma_{11}\rangle_\Omega} \end{cases} \tag{28}$$

$$\mathcal{E} = \lfloor 0 \quad \beta \quad 0 \rfloor^{\mathrm{T}} \rightarrow \begin{cases} E^* = \dfrac{\left(3\langle\sigma_{11}\rangle_\Omega - \langle\sigma_{22}\rangle_\Omega\right)}{\left(\langle\sigma_{11}\rangle_\Omega - \langle\sigma_{22}\rangle_\Omega\right)\beta}\langle\sigma_{22}\rangle_\Omega \\ v^* = -\dfrac{\langle\sigma_{11}\rangle_\Omega}{\langle\sigma_{11}\rangle_\Omega - \langle\sigma_{22}\rangle_\Omega} \end{cases} \tag{29}$$

while for plane stress state the equations remain as in Eqs. 18 and 19.

Application examples

In order to assert the validity of the proposed methodology, some examples are presented in this section. First, a statistical analysis is performed for a virtual material to determine the size of the RVE, following [9]. The microstructure topology is similar to the nodular cast iron (NCI). The effective properties of the material are then estimated. The second example shows the results obtained with the present formulation for a plate containing a uniform array of the holes. These results are compared to the numerical and experimental works of references [19] and [20], respectively.

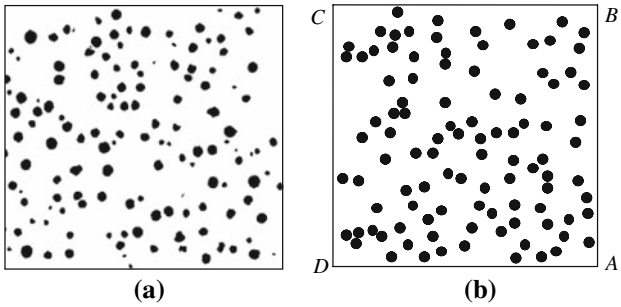

Fig. 2 Micro-porous material. (**a**) Typical micrograph sample of an ADI (150 nodules/mm^2). (**b**) Numerical model (volume fraction of 7.7% and an average ratio $R/d = 0.25$–140 voids)

Example 1: NCI RVE analysis

Following [21–23], a homogenized microstructure is analyzed under plane stress state. Figure 2a shows a typical micrograph of the spheroidal graphite cast iron studied. The material matrix is considered ferritic. From the work of [24], the properties of the ferritic matrix are set with $E_m = 210$ GPa and $v_m = 0.3$. The R/d is used as the characteristic parameter, where R is the average void radius and d the average minimum distance between void centers. In [25], a statistical analysis of measurements performed on standard NCI micrographs using image-processing software is accomplished. The results obtained for the R/d parameter are shown in Table 1. It can be seen that for a wide range of nodular counts, ranging from 60 to 600 nodules/mm^2, R/d and its standard deviation are almost constant with $R/d = 0.25$ and a standard deviation of 35%. In all cases, there is 100% of nodularity (i.e., all graphite is in the form of roughly equiaxed nodules). The graphite nodules volume fraction is 7.7%.

The numerical model was built by generating the holes at random locations, checking for superposition and matching

Table 1 Results of statistical analysis performed on standard ADI micrographs [25]

Nodules/area (mm^{-2})	Nodularity (%)	R/d (average)	Standard deviation (%)
60	100	0.27682	31.18
100	100	0.26175	37.56
150	100	0.25294	35.43
600	100	0.25625	32.62

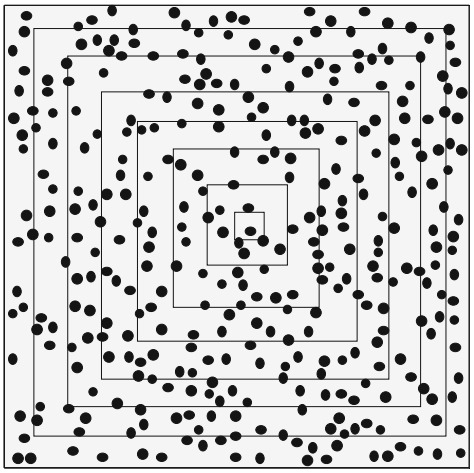

Fig. 3 Comparative visualization of the microstructure models used to determine the RVE size

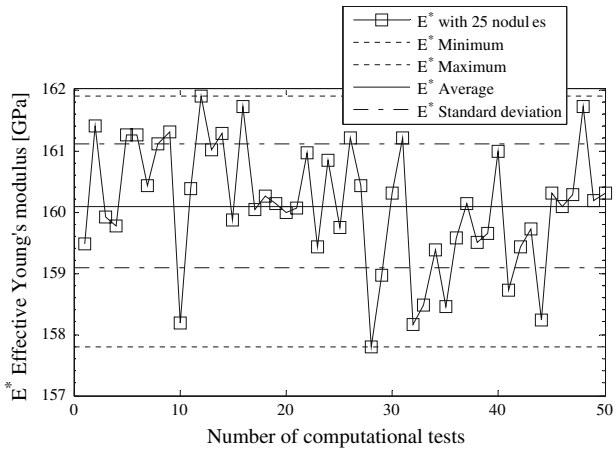

Fig. 4 Effective Young's modulus for 50 microstructures containing 25 voids randomly distributed in each case. The maximum, minimum, average, and standard deviation values are indicated

the experimental distribution data. An example is depicted in Fig. 2b. Since there is no standard procedure to determine directly the dimensions or number of heterogeneities to be included in the RVE, the dimensions of the RVE are determined in a numerical way through successive increments of the sample volume. The representative size of the sample is such that it provides an invariant macroscopic response (within certain bounds) for different distributions of inhomogeneities. Figure 3 illustrates different microstructure samples used to determine the RVE size.

Fifty samples are simulated to study the effective response of the microstructure, each one with a different random distribution of voids. The 4-node hole boundary element [14] was used to model the micro-void. Figures 4 and 5 present the results obtained for E^* and ν^*, respectively (Eqs. 18 or 19), with samples containing 25 voids in all cases. Each point in these figures represents the result of a computational test.

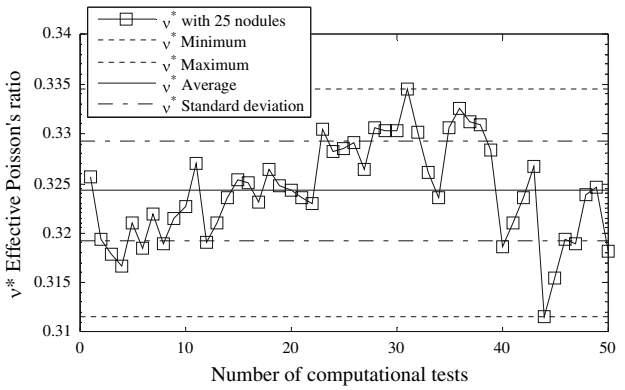

Fig. 5 Effective Poisson's ratio for 50 microstructures containing 25 voids randomly distributed in each case. The maximum, minimum, average, and standard deviation values are indicated

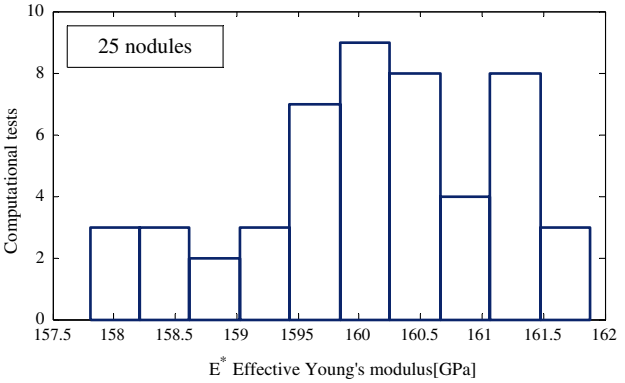

Fig. 6 Histogram of the effective Young's modulus (GPa) for 50 microstructure with 25 voids randomly distributed in each case

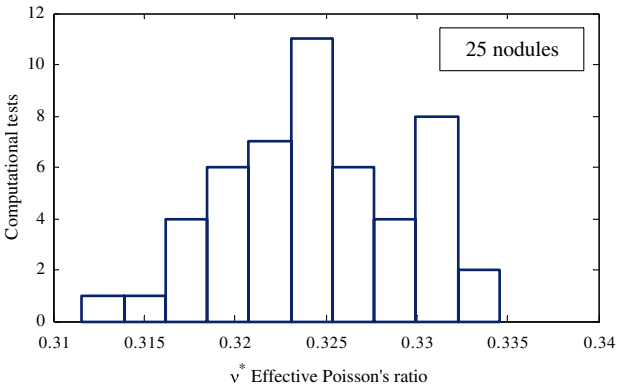

Fig. 7 Histogram of the effective Poisson's ratio for 50 microstructure with 25 voids randomly distributed in each case

Also observed are the maximum, minimum, average, and standard deviation of the group of samples. Figures 6 and 7 depict the corresponding histograms of these results. The simulations were carried out for microstructures containing 2, 4, 6, 8, 10, 15, 20, 25, 30, 40, 50, and 60 voids in order to establish the RVE size. In all cases 50 computational tests were performed. The results obtained are presented in Fig. 8

for the E^*, while the results for v^* are shown in Fig. 9. Tables 2 and 3 summarize the statistical information of the samples as average values of the effective mechanical properties, difference between maximum and minimum and standard deviation. The percentage deviation of these values from the average is also presented.

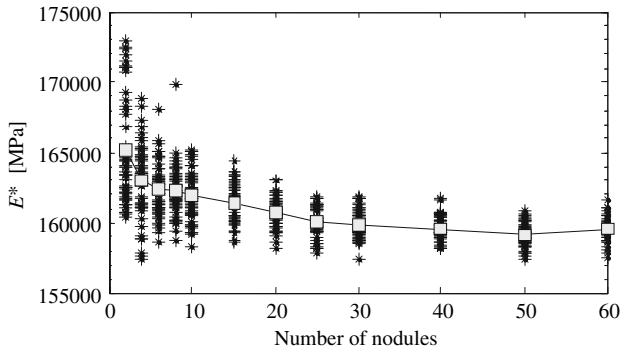

Fig. 8 Convergence curve of the RVE. Values of the effective Young's modulus for samples with different random distributions of voids

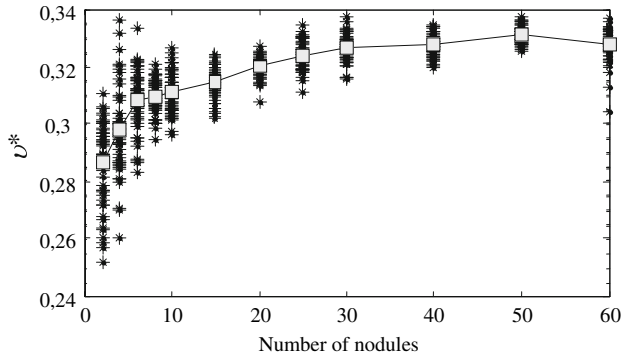

Fig. 9 Convergence curve of the RVE. Values of the effective Poisson's ratio for samples with different random distributions of voids

These results points out that a micro-structured material sample containing 25 voids is adequate to generate effective properties within approximate error bounds of 2.5% for E^* and 6.5% for v^*.

It is also interesting to compare of these results with analytical methods based on the consideration of a single inhomogeneity in an unbounded domain (see, for instance [9, 10, 26]). Table 4 shows the estimated properties for the *diluted distribution* (DD), *Mori-Tanaka* (MT), and the *self-consistent* (SC) methods along with the averaged results obtained through the present methodology using 25 voids. In all cases, a plate with circular voids under plane stress and macroscopic isotropic behavior are considered. While the SC approach supplies the best agreement for that particular volume fraction, all methods predict stiffer properties.

In order to illustrate the significant reduction in the number of degrees of freedom when the proposed hole element is used in the numerical model, a particular microstructure topology is conventionally discretized with discontinuous quadratic elements and a convergence study is carried out. The sample contains 25 voids randomly distributed. Figures 10–12 show the effective properties and the strain energy (evaluated as $\frac{1}{2}\langle\sigma_{ij}\rangle_\Omega\langle\varepsilon_{ij}\rangle_\Omega$) convergence obtained using progressively finer conventional meshes ($\square$) and using the present 3, 4, 5, and 6-noded hole elements ($\triangle$). Table 5 reports the relative error for the various hole elements when compared to the conventional BEM using the finest mesh from Figs. 10–12 (2,784 degrees of freedom). In all cases the error does not exceed 0.35%. As expected, the best performance corresponds to the 6-noded element. One should note, however, that the lower order elements may be computationally more economical in practical cases containing many voids, since in such cases a lower number of nodes is be enough to describe the deformation of the voids.

Table 2 Numerical results for Young's modulus on simulated microstructures with various random distributions of voids

Number of voids	E^*_{avg} (MPa)	$E^*_{max} - E^*_{min}$ (MPa)	Standard deviation	$\frac{E^*_{max}-E^*_{min}}{E^*_{avg}} \times 100$ (%)	$\frac{\text{Standard deviation}}{E^*_{avg}} \times 100$ (%)
2	165,129	12,450	3,932	7.54	2.38
4	163,019	11,388	2,661	6.99	1.63
6	162,331	9,380	1,904	5.78	1.17
8	162,237	11,032	1,762	6.80	1.09
10	161,955	6,860	1,756	4.24	1.08
15	161,437	5,736	1,406	3.55	0.87
20	160,713	4,840	1,018	3.01	0.63
25	160,096	4,077	988	2.55	0.62
30	159,910	4,447	994	2.78	0.62
40	159,622	3,550	868	2.22	0.54
50	159,163	3,415	820	2.15	0.52
60	159,575	4,106	819	2.57	0.51

Table 3 Numerical results for Poisson's ratio on simulated microstructures with various random distributions of voids

Number of voids	v^*_{avg}	$v^*_{max} - v^*_{min}$	Standard deviation	$\frac{v^*_{max}-v^*_{min}}{v^*_{avg}} \times 100$ (%)	$\frac{\text{Standard deviation}}{v^*_{avg}} \times 100$ (%)
2	0.287	0.059	0.015	20.38	5.16
4	0.298	0.076	0.016	25.43	5.21
6	0.309	0.050	0.011	16.22	3.47
8	0.310	0.026	0.006	8.53	1.89
10	0.311	0.030	0.007	9.74	2.29
15	0.315	0.022	0.006	7.13	1.83
20	0.320	0.019	0.004	6.07	1.15
25	0.324	0.021	0.005	6.46	1.48
30	0.327	0.021	0.004	6.50	1.35
40	0.328	0.015	0.004	4.64	1.15
50	0.331	0.011	0.003	3.43	0.85
60	0.328	0.032	0.006	9.85	1.75

Table 4 Comparison of various methods to estimate effective properties

	E^* (MPa)	μ^* (MPa)	ν^*
Dilute distribution	$E^*_{DD} = \frac{E_m}{1+3\phi} = 170,593$	$\mu^*_{DD} = \frac{E_m}{2(1+\nu_m+4\phi)} = 65,298$	0.306
Mori-Tanaka	$E^*_{MT} = \frac{E_m(1-\phi)}{1+2\phi} = 167,963$	$\mu^*_{MT} = \frac{\mu_m(1-\phi)(1+\nu_m)}{1+\nu_m+\phi(3-\nu_m)} = 64,271$	0.307
Self-consistent	$E^*_{SC} = E_m(1-3\phi) = 161,490$	$\mu^*_{SC} = \frac{E_m(1-3\phi)}{2[1+\phi+\nu_m(1-3\phi)]} = 61,745$	0.308
Present work	160,096	60,459	0.324

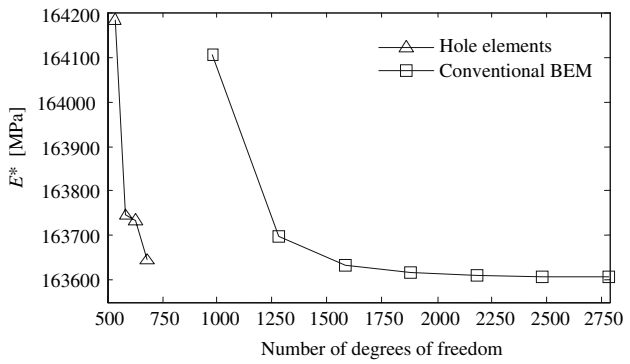

Fig. 10 Convergence of the effective Young's modulus

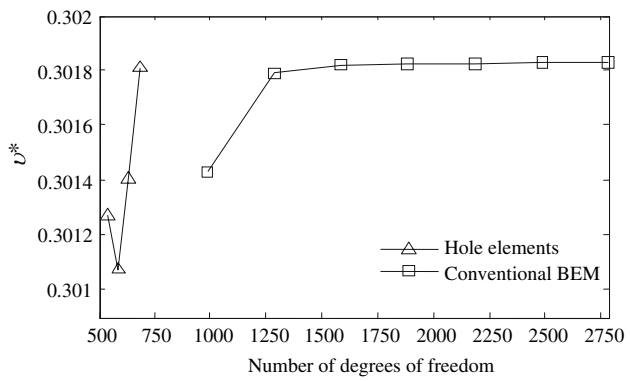

Fig. 11 Convergence of the effective Poisson's ratio

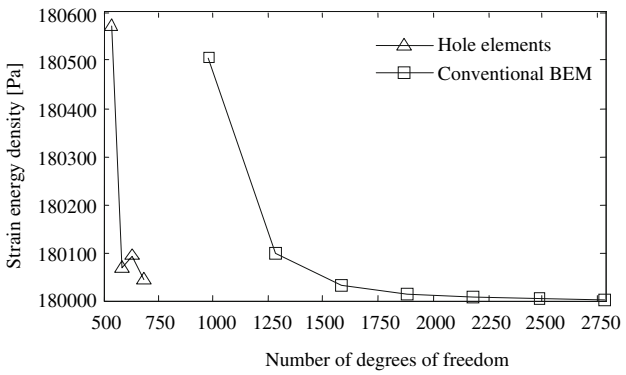

Fig. 12 Convergence of the effective strain energy

Example 2: plate with uniform array of holes

In this example, the microstructure is composed by a periodic pattern of regularly spaced voids. A drawing of the test specimen and the characteristic dimensions of the unit cell structure are depicted in Fig. 13. Experimental results for an Aluminum plate with the same configuration submitted to axial loadings are available [20]. The material used has $E_m = 72{,}700$ MPa and $\nu_m = 0.34$. The thickness of the plate is $t = 2$ mm and the distance between a hole near the free surface and the edge is $t/2-R$. The effective Young's modulus for a specimen with 25 holes (volume fraction of $\phi_1 = 0.0707$) is 59,259 MPa, while the

Table 5 Relative errors of the hole element. $(\cdot)_{BEM}$ refers to the results obtained using conventional hole discretization with 16 quadratic elements

Type of boundary element	Relative error of effective Young's modulus $\left\lvert\frac{E^*_{\text{hole element}}-E^*_{BEM}}{E^*_{BEM}}\right\rvert \times 100$ (%)	Relative error of effective Poisson's ratio $\left\lvert\frac{\nu^*_{\text{hole element}}-\nu^*_{BEM}}{\nu^*_{BEM}}\right\rvert \times 100$ (%)	Relative error of effective strain energy $U^*\left\lvert\frac{U^*_{\text{hole element}}-U^*_{BEM}}{U^*_{BEM}}\right\rvert \times 100$ (%)
3-noded	0.35	0.185	0.317
4-noded	0.086	0.25	0.036
5-noded	0.078	0.14	0.05
6-noded	0.024	0.007	0.023

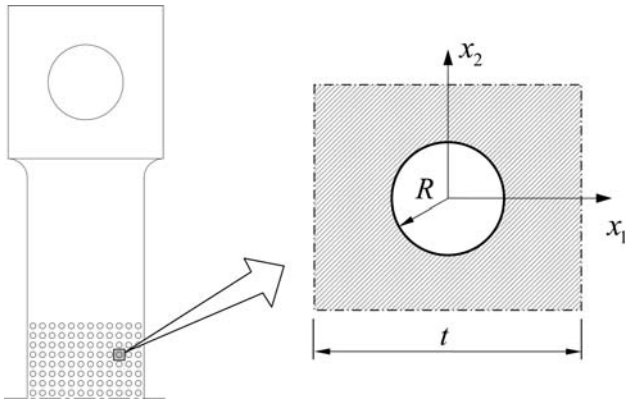

Fig. 13 Representation of the unit cell from a test specimen [20]

corresponding values for a specimen with 121 holes (volume fraction $\phi_2 = 0.3848$) is 26,531 MPa.

A plane stress model with 6-noded hole elements was used for each case. Note that the microstructure has orthotropic geometric symmetry but in this particular case, the effective Young's moduli are the same in x_1 and x_2 directions and then Eqs. (18) and (19) can be used. The estimated effective Young's moduli obtained are 56,692 and 28,340 MPa for ϕ_1 and ϕ_2 volume fractions, respectively. In Table 6, these results are presented with analytical predictions and Dong's [19] numerical results for the same unit cell but a different Poisson's ratio.

Conclusions

A general procedure for estimation of effective properties of micro-structured materials containing randomly distributed cylindrical voids has been presented. The procedure combines the average field theory and statistical analysis with the boundary element method. The standard boundary element formulation is used to model the outer matrix boundary, while a special *hole* boundary element is employed to model each void. This approach is particularly suitable to solve repetitive problems with a large number of voids, such as the typical ones found in RVE analysis, since the amount of data and computational cost is drastically reduced. In addition, the microstructure discretization strategy becomes rather simple when compared to the conventional BEM or other discretization methods. The scheme preserves the BEM computational advantage by using boundary-only data. A natural follow on this topic is the derivation of a spherical hole element for three-dimensional analysis, and the present work provides a starting point towards such element, since all it is needed is a double integration over the surface of the element, instead of our single integration over the perimeter of the hole.

Expressions for effective properties in function of the micro-fields both for isotropic and transversally isotropic hypothesis have been derived.

Application examples have been illustrated by estimating the effective elastic properties of a micro-structured material with holes distribution taken from NCI samples and from a plate containing uniform array of holes. The results have shown good agreement with those available from the literature.

The proposed approach has great potential to be used for modeling problems with non-linear behavior, as well as problems with high volume fraction, when many of the available analytic models fail. Some further improvements can be addressed, like the use of fast multipole techniques [27, 28] to analyze large-scale problems. Furthermore, the formulation can be straightforwardly extended to three-dimensional problems.

Table 6 Comparative values of E^*/E_m

Volume fraction	E^*/E_m			
	Hole element ($\nu_m = 0.34$)	Experimental ($\nu_m = 0.34$)	Analytical	Dong [19] ($\nu_m = 0.3$)
0.0707	0.78	0.815	0.788 (self-consistent)	0.824
0.3848	0.39	0.365	0.348 (Mori-Tanaka)	0.407

Acknowledgements The first author wishes to express his gratitude to CNPq (Brazil) for the financial support and to Prof. Adrián P. Cisilino (National University of Mar del Plata, Argentina) for useful discussions. The authors are also grateful to Prof. V. Mantič for his comments on the original manuscript. This work was partially financed by PROSUL 490185/2005-3 and CAPES/SECYP 048/03 projects.

Appendix

The shape functions used by the hole elements are presented below.

- 3-noded element (as proposed by Henry and Banerjee [4]):

$$M_1(\theta) = \frac{1}{3} + \frac{2}{3}\cos\theta$$
$$M_2(\theta) = \frac{1}{3} + \frac{\sqrt{3}}{3}\sin\theta - \frac{1}{3}\cos\theta$$
$$M_3(\theta) = \frac{1}{3} - \frac{\sqrt{3}}{3}\sin\theta - \frac{1}{3}\cos\theta$$

- 4-noded element:

$$M_1(\theta) = \frac{(1+\cos\theta)}{2}\cos\theta$$
$$M_2(\theta) = \frac{1}{2} + \frac{1}{2}\sin\theta - \frac{1}{2}\cos^2\theta$$
$$M_3(\theta) = \frac{(-1+\cos\theta)}{2}\cos\theta$$
$$M_4(\theta) = \frac{1}{2} - \frac{1}{2}\sin\theta - \frac{1}{2}\cos^2\theta$$

- 5-noded element:

$$M_1(\theta) = \frac{\cos^2\theta + \cos\left(\frac{\pi}{5}\right)\cos\theta - \cos\left(\frac{2\pi}{5}\right)\cos\theta - \cos\left(\frac{\pi}{5}\right)\cos\left(\frac{2\pi}{5}\right)}{\cos\left(\frac{\pi}{5}\right)\cos\left(\frac{2\pi}{5}\right) - \cos\left(\frac{\pi}{5}\right) + \cos\left(\frac{2\pi}{5}\right) - 1}$$

$$M_2(\theta) = \frac{\cos\left(\frac{2\pi}{5}\right)\cos\theta\sin\theta - \cos\left(\frac{\pi}{5}\right)\sin\theta + \cos\left(\frac{\pi}{5}\right)\cos\left(\frac{2\pi}{5}\right)\sin\theta - \cos\theta\sin\theta}{\Psi} + \frac{\sin\left(\frac{2\pi}{5}\right)\cos^2\theta - \sin\left(\frac{2\pi}{5}\right)\cos\theta + \sin\left(\frac{2\pi}{5}\right)\cos\left(\frac{\pi}{5}\right)\cos\theta - \sin\left(\frac{2\pi}{5}\right)\cos\left(\frac{\pi}{5}\right)}{\Psi}$$

$$M_3(\theta) = \frac{\cos\left(\frac{2\pi}{5}\right)\cos\left(\frac{\pi}{5}\right)\sin\theta + \cos\left(\frac{2\pi}{5}\right)\sin\theta - \cos\left(\frac{\pi}{5}\right)\cos\theta\sin\theta - \cos\theta\sin\theta}{\Sigma} + \frac{\sin\left(\frac{\pi}{5}\right)\cos^2\theta - \sin\left(\frac{\pi}{5}\right)\cos\left(\frac{2\pi}{5}\right)\cos\theta - \sin\left(\frac{\pi}{5}\right)\cos\theta + \sin\left(\frac{\pi}{5}\right)\cos\left(\frac{2\pi}{5}\right)}{\Sigma}$$

$$M_4(\theta) = \frac{-\cos\left(\frac{2\pi}{5}\right)\cos\left(\frac{\pi}{5}\right)\sin\theta - \cos\left(\frac{2\pi}{5}\right)\sin\theta + \cos\left(\frac{\pi}{5}\right)\cos\theta\sin\theta + \cos\theta\sin\theta}{\Sigma} + \frac{\sin\left(\frac{\pi}{5}\right)\cos^2\theta - \sin\left(\frac{\pi}{5}\right)\cos\left(\frac{2\pi}{5}\right)\cos\theta - \sin\left(\frac{\pi}{5}\right)\cos\theta + \sin\left(\frac{\pi}{5}\right)\cos\left(\frac{2\pi}{5}\right)}{\Sigma}$$

$$M_5(\theta) = \frac{-\cos\left(\frac{2\pi}{5}\right)\cos\left(\frac{\pi}{5}\right)\sin\theta - \cos\left(\frac{2\pi}{5}\right)\sin\theta\cos\theta + \cos\left(\frac{\pi}{5}\right)\sin\theta + \cos\theta\sin\theta}{\Psi} + \frac{\sin\left(\frac{2\pi}{5}\right)\cos^2\theta + \sin\left(\frac{2\pi}{5}\right)\cos\left(\frac{\pi}{5}\right)\cos\theta - \sin\left(\frac{2\pi}{5}\right)\cos\theta - \sin\left(\frac{2\pi}{5}\right)\cos\left(\frac{\pi}{5}\right)}{\Psi}$$

where

$$\Psi = 2\sin\left(\frac{2\pi}{5}\right)\left[\cos^2\left(\frac{2\pi}{5}\right) - \cos\left(\frac{2\pi}{5}\right) + \cos\left(\frac{2\pi}{5}\right)\cos\left(\frac{\pi}{5}\right) - \cos\left(\frac{\pi}{5}\right)\right]$$

$$\Sigma = 4\sin\left(\frac{\pi}{5}\right)\left[\cos^2\left(\frac{\pi}{5}\right) + \cos\left(\frac{2\pi}{5}\right) + \cos\left(\frac{2\pi}{5}\right)\cos\left(\frac{\pi}{5}\right) + \cos\left(\frac{\pi}{5}\right)\right]$$

- 6-noded element:

$$M_1(\theta) = -\frac{1}{6} - \frac{1}{6}\cos\theta + \frac{2}{3}\cos^2\theta + \frac{2}{3}\cos^3\theta$$

$$M_2(\theta) = \frac{\sqrt{3}}{6}\sin\theta + \frac{\sqrt{3}}{3}\sin\theta\cos\theta - \frac{1}{3}\cos^2\theta - \frac{2}{3}\cos^3\theta + \frac{2}{3}\cos\theta + \frac{1}{3}$$

$$M_3(\theta) = \frac{\sqrt{3}}{6}\sin\theta - \frac{\sqrt{3}}{3}\sin\theta\cos\theta - \frac{2}{3}\cos\theta - \frac{1}{3}\cos^2\theta + \frac{2}{3}\cos^3\theta + \frac{1}{3}$$

$$M_4(\theta) = -\frac{1}{6} + \frac{1}{6}\cos\theta + \frac{2}{3}\cos^2\theta - \frac{2}{3}\cos^3\theta$$

$$M_5(\theta) = -\frac{\sqrt{3}}{6}\sin\theta + \frac{\sqrt{3}}{3}\sin\theta\cos\theta - \frac{2}{3}\cos\theta - \frac{1}{3}\cos^2\theta + \frac{2}{3}\cos^3\theta + \frac{1}{3}$$

$$M_6(\theta) = -\frac{\sqrt{3}}{6}\sin\theta - \frac{\sqrt{3}}{3}\sin\theta\cos\theta + \frac{2}{3}\cos\theta - \frac{1}{3}\cos^2\theta - \frac{2}{3}\cos^3\theta + \frac{1}{3}$$

The shape functions for 4, 5, and 6-noded elements were proposed in [13]. It is important to point out that all the functions describe exactly rigid body movements of the holes.

References

1. Hu N, Wang B, Tan GW, Yao ZH, Yuan WF (2000) Compos Sci Technol 60:1811
2. Yang Q-S, Qin Q-H (2004) Eng Anal Bound Elem 28:919
3. Dong CY, Lee KY (2006) Eng Anal Bound Elem 30:662
4. Okada H, Fukui Y, Kumazawa N (2001) Comput Struct 79:1987
5. Dong CY, Lo SH, Cheung YK (2002) Eng Anal Bound Elem 26:471
6. Knight MG, Wrobel LC, Henshall JL (2003) Compos Struct 62:341
7. Wang J, Crouch SL, Mogilevskaya SG (2003) Eng Anal Bound Elem 27:789
8. Mogilevskaya SG, Crouch SL (2001) Int J Numer Meth Eng 52:1069
9. Zohdi TI (2002) In: Computational modeling and design of new random microheterogeneous materials. CISM Course notes, Udine Italy
10. Nemat-Nasser S, Hori M (1999) In: Micromechanics: overall properties of heterogeneous solids. Elsevier
11. Hori M, Nemat-Nasser S (1999) Mech Mater 31:667
12. Henry DP, Banerjee PK (1991) Int J Numer Meth Eng 31:369
13. Buroni FC, Marczak RJ (2006) In: Cardona A, Nigro N, Songzogni V, Storti M (eds) Mecánica Computacional, vol XXV. Santa Fé, Argentina, p 2747
14. Buroni FC, Marczak RJ (2007) A family of hole boundary elements for modeling materials with cylindrical voids. Accepted in: Eng Anal Bound Elem. doi:10.1016/j.enganabound.2007.11.003
15. Buroni FC, Marczak RJ (2006) In: Cardona A, Nigro N, Songzogni V, Storti M (eds) Mecánica computacional, vol XXV. Santa Fé, Argentina, p 2835
16. Banerjee PK (1994) In: The boundary element methods in engineering. Mc Graw-Hill
17. Brebbia CA, Dominguez J (1992) Boundary elements. An introductory course. Computational Mechanics Publications. McGraw-Hill
18. Kanit T, Forest S, Galliet I, Mounoury V, Jeulin D (2003) Int J Solids Struct 40:3647
19. Dong CY (2006) Int J Solids Struct 43:7919
20. Öchsner A (2004) Numerical simulation of the mechanical behavior of cellular materials. Research report, Mechanical Engineering Department, Universidade de Aveiro, Portugal
21. Batista RG, Cisilino AP, Iturrioz I (2003) In: Rosales MB, Cortínez VH, Bambill DV (eds) Mecánica computacional, vol XXII. p 1878
22. Pundale SH, Rogers RJ, Nadkarni GR (1998) Am Foundrymen Soc Trans 106:99
23. Berdin C, Dong MJ, Prioul C (2001) Eng Fract Mech 68:1107
24. Zhang KS, Bai JB, François D (1999) Int J Solids Struct 36:3407
25. Ortiz JE, Cisilino AP, Otegui JL (2001) Fatigue Fract Engng Mater Struct 24:591
26. Gross D, Seelig T (2006) In: Fracture mechanics with an introduction to micromechanics. Springer
27. Rokhlin V (1985) J Comput Phys 60:187
28. Fu YH, Klimkowski KJ, Rodin GJ, Berger E, Browne JC, Singer JK, Geijn RA (1998) Int J Numer Meth Eng 42:1215